

Noise Suppression Detection Method Based on Time Reversed Signal Waveform Similarity

Bing Li

School of Electrical Engineering
Southwest Jiaotong University, Chengdu 610031, China
blijess@outlook.com

Abstract — A novel time reversal detection (TRD) algorithm for noise suppression is presented. The targets can be located accurately by analyzing the cross-correlation character of TR echo signals received by sub-arrays. Compared with conventional TR algorithm, the performance of proposed method is superior, especially under low signal-to-noise ratio (SNR) condition.

Index Terms — Cross-correlation, noise suppression, sub-arrays, time reversal.

I. INTRODUCTION

Time-reversal (TR) methods have attracted much significant attention and interest recently due to their promising use in a wide range of applications. Its basic principle is able to be described as follows: firstly, the channel state information can be extracted by observing the received signal from the sources or scatterers; then, this received signal is time-reversed in time domain (or phase conjugated in the frequency domain) and retransmitted from the respective receiver used as transmitter in this stage; finally, according to the spatial reciprocity principle, the rebroadcast wavefields focus at the locations of the original sources or scatterers. This effect is valuable for many applications in which the energy of acoustic or electromagnetic waves needs to be physically focused at the desired destination, e.g., in communications or biomedical applications [1-4].

Most current TR methods require a large number of echo signals, such as the time reversal multiple-signal-classification (TR-MUSIC) algorithm and decomposition of the time-reversal operator (DORT), these two algorithms need to measure $N \times N$ echo signals for constructing the multistatic data matrix (MDM) whose size is $N \times N$, where N is the total number of transceivers [5-8]. Moreover, the conventional TR method also needs to measure a lot of echo signals for improving TR-focusing quality (resolution) and suppressing noise interference.

TR system becomes more practical, low cost and exploitable if few echo signals can be successfully utilized, since making use of few echo signals purports

to employ few detection elements [9]. However, when few echo signals are used, the MDM may be unavailable, or multiple spurious images which can be misinterpreted as scatterers may be appearance under noisy conditions.

To address the aforementioned issues, I propose a new TRD approach which can suppress incoherent noise effectively. The general idea of this new approach is as follows: firstly, the detection array is divided into several looks (sub-arrays). Secondly, the echoes received by each sub-array are separately time reversed. Finally, the detection map is able to be obtained by calculating the cross-correlation of TR signals of the sub-arrays. Since the noise is irrelevant to the TR-focusing signal, the proposal method can effectively suppress the noise, even in a situation where few echo signals are available.

Furthermore, the TR signal is easy to be interfered by noise in a simple environment, since the TR-focusing effect gets weak. In contrast, the TR-focusing effect can be strengthened in the cluttered environment where the focal signal can be improved. Therefore, the detection method which works well to suppress noise in the simple environment is able to have a better performance in the cluttered environment. As a result, in this study, an experiment was arranged to investigate the proposal algorithm in a simple environment [8].

It is worthwhile mean that, in order to estimate the impact of noise on the algorithm accurately, the measured experiment was taken in a microwave chamber to obtain low-noise echo signals. And then an extra additive white Gaussian noise is added to the low-noise echoes, so as to obtain the high-noise echo signals. And this additive white Gaussian noise is a good candidate to simulate background noise, thermal noise, inner noise of system, etc. and is often assumed to be zero mean in the image denoising literature [10].

II. NOVEL TRD METHOD

Assume a target located at \mathbf{r}_s , an array of N transceivers, and the n th transceiver's receiver and transmitter separately located at \mathbf{r}_n and \mathbf{r}'_n . A time domain probing pulse $x(t)$ is emitted from the n th

transmitter. The Fourier transform of incident signal at the target's location can be represented as:

$$S(\omega, \mathbf{r}_s) = G(\mathbf{r}_s, \mathbf{r}'_n, \omega) X(\omega), \quad (1)$$

where $X(\omega)$ is the Fourier transform of $x(t)$ and $G(\mathbf{r}_s, \mathbf{r}'_n, \omega)$ is the background Green function that satisfies the reduced wave equation [11] representing the "propagator" from location \mathbf{r}'_n to \mathbf{r}_s . In the presence of additive white Gaussian noise $w_n(t)$ which is called noise for short thereafter, the signal received by the corresponding receiver at \mathbf{r}_n could be modeled as:

$$\mathbf{y}(t, \mathbf{r}_n, \mathbf{r}'_n) = \frac{1}{2\pi} \int [G(\mathbf{r}_n, \mathbf{r}_s, \omega) G(\mathbf{r}_s, \mathbf{r}'_n, \omega) X(\omega) + W_n(\omega)] e^{i\omega t} d\omega, \quad (2)$$

where $W_n(\omega)$ is the Fourier transform of $w_n(t)$.

Since a TR signal in time domain is equivalent to taking the complex conjugate in frequency domain, the TR version of this response becomes, with the length of the time-window being denoted as T ,

$$\mathbf{y}_{TR}(T-t, \mathbf{r}_n, \mathbf{r}'_n) = \frac{1}{2\pi} \int [G^*(\mathbf{r}_n, \mathbf{r}_s, \omega) G^*(\mathbf{r}_s, \mathbf{r}'_n, \omega) X^*(\omega) + W_n^*(\omega)] e^{-i\omega T} e^{i\omega t} d\omega, \quad (3)$$

where "*" represents the complex conjugate.

Accounting for propagation from the n th transmitter at \mathbf{r}'_n and the n th receiver at \mathbf{r}_n to any point at \mathbf{r}_k in the detection domain, the TR signal for a generic observation point \mathbf{r}_k can be illustrated as:

$$f(t, \mathbf{r}_k, \mathbf{r}_n, \mathbf{r}'_n) = \frac{1}{2\pi} \int [G^*(\mathbf{r}_n, \mathbf{r}_s, \omega) G^*(\mathbf{r}_s, \mathbf{r}'_n, \omega) X^*(\omega) + W_n^*(\omega)] \times G(\mathbf{r}_k, \mathbf{r}'_n, \omega) G(\mathbf{r}_n, \mathbf{r}_k, \omega) e^{-i\omega T} e^{i\omega t} d\omega. \quad (4)$$

In the proposal method, the transceivers are divided into several sub-arrays (looks), before the received signals are time reversed and resubmitted. Assume each sub-array includes L adjacent transceivers. Therefore, the number of sub-arrays is $N-L+1$. According to (4), at point \mathbf{r}_k , the TR signal of the a th sub-array containing transceivers $n_a \dots n_a + L - 1$ is:

$$\begin{aligned} f_a(t, \mathbf{r}_k) &= \sum_{n=n_a}^{n_a+L-1} f(t, \mathbf{r}_k, \mathbf{r}_n, \mathbf{r}'_n) \\ &= \frac{1}{2\pi} \int \sum_{n=n_a}^{n_a+L-1} G^*(\mathbf{r}_n, \mathbf{r}_s, \omega) G^*(\mathbf{r}_s, \mathbf{r}'_n, \omega) G(\mathbf{r}_k, \mathbf{r}'_n, \omega) \\ &\quad \times G(\mathbf{r}_n, \mathbf{r}_k, \omega) X^*(\omega) e^{-i\omega T} e^{i\omega t} d\omega \\ &\quad + \frac{1}{2\pi} \int \sum_{n=n_a}^{n_a+L-1} G(\mathbf{r}_k, \mathbf{r}'_n, \omega) G(\mathbf{r}_n, \mathbf{r}_k, \omega) W_n^*(\omega) e^{-i\omega T} e^{i\omega t} d\omega \\ &= v_a(t, \mathbf{r}_k) + u_a(t, \mathbf{r}_k), \end{aligned} \quad (5)$$

where

$$v_a(t, \mathbf{r}_k) = \frac{1}{2\pi} \int \sum_{n=n_a}^{n_a+L-1} G^*(\mathbf{r}_n, \mathbf{r}_s, \omega) G^*(\mathbf{r}_s, \mathbf{r}'_n, \omega) G(\mathbf{r}_k, \mathbf{r}'_n, \omega) \times G(\mathbf{r}_n, \mathbf{r}_k, \omega) X^*(\omega) e^{-i\omega T} e^{i\omega t} d\omega, \quad (6)$$

$$u_a(t, \mathbf{r}_k) = \frac{1}{2\pi} \int \sum_{n=n_a}^{n_a+L-1} G(\mathbf{r}_k, \mathbf{r}'_n, \omega) G(\mathbf{r}_n, \mathbf{r}_k, \omega) W_n^*(\omega) e^{-i\omega T} e^{i\omega t} d\omega. \quad (7)$$

Likewise, $f_b(t, \mathbf{r}_k)$, $v_b(t, \mathbf{r}_k)$ and $u_b(t, \mathbf{r}_k)$ can be got in the same way, and calculate the cross-correlation function between $f_a(t, \mathbf{r}_k)$ and $f_b(t, \mathbf{r}_k)$,

$$\begin{aligned} D_p(t, \mathbf{r}_k) &= \int_{-\infty}^{\infty} f_a^*(\tau, \mathbf{r}_k) f_b(t+\tau, \mathbf{r}_k) d\tau \\ &= \int_{-\infty}^{\infty} v_a^*(\tau, \mathbf{r}_k) v_b(t+\tau, \mathbf{r}_k) d\tau + \int_{-\infty}^{\infty} u_a^*(\tau, \mathbf{r}_k) v_b(t+\tau, \mathbf{r}_k) d\tau \\ &\quad + \int_{-\infty}^{\infty} v_a^*(\tau, \mathbf{r}_k) u_b(t+\tau, \mathbf{r}_k) d\tau + \int_{-\infty}^{\infty} u_a^*(\tau, \mathbf{r}_k) u_b(t+\tau, \mathbf{r}_k) d\tau. \end{aligned} \quad (8)$$

Then, the target image can be built by using the following function:

$$I(\mathbf{r}_k) = \sum_{p=1}^{C(N-L+1, 2)} |D_p(0, \mathbf{r}_k)|, \quad (9)$$

where $C(N-L+1, 2)$ is the number of 2-combinations from $N-L+1$ elements. Due to the space focusing and temporal compression of TR signal at point \mathbf{r}_s , $f_a(t, \mathbf{r}_k)$ is similar to $f_b(t, \mathbf{r}_k)$ near the time reference $t=T$. Therefore, according to Equation (8), the maximum value of cross-correlation function can be obtained at $t=0$. Furthermore, at the point \mathbf{r}_k ($\mathbf{r}_k \neq \mathbf{r}_s$), $f_a(t, \mathbf{r}_k)$ is irrelevant to $f_b(t, \mathbf{r}_k)$. That means the value of cross-correlation function at the point \mathbf{r}_s are larger than those at off-target points, namely, $|D_p(0, \mathbf{r}_s)| > |D_p(0, \mathbf{r}_k)|$, ($\mathbf{r}_k \neq \mathbf{r}_s$). With the use of Equation (9), the detection map is built, and the point with the maximum value is the position of target.

In addition, $u_a(t, \mathbf{r}_k)$ and $u_b(t, \mathbf{r}_k)$ are random and uncorrelated, that means,

$$\int_{-\infty}^{\infty} u_a^*(\tau, \mathbf{r}_k) u_b(\tau, \mathbf{r}_k) d\tau \cong 0. \quad (10)$$

And the TR echo signals without noise are irrelevant to noise. Therefore, we can get

$$\begin{cases} \int_{-\infty}^{\infty} u_a^*(\tau, \mathbf{r}_k) v_b(\tau, \mathbf{r}_k) d\tau \cong 0 \\ \int_{-\infty}^{\infty} v_a^*(\tau, \mathbf{r}_k) u_b(\tau, \mathbf{r}_k) d\tau \cong 0 \end{cases}. \quad (11)$$

Furthermore, the impacts of noise on the reconstructed image $I(\mathbf{r}_k)$ can be neglected. In other words, the proposed method can effectively suppress the noise interference.

III. EXPERIMENT AND DISCUSSION

To verify and investigate the performance of the proposed method, two experiments were taken. Firstly, a numerical experiment was taken to investigate the availability of sub-arrays' constitution. Then, a measured experiment was executed to prove the feasibility of the proposed method in the applications where few echo signals were used.

A. Numerical experiment

In this section, The Gaussian modulated pulse of 0.5-ns duration centered at 3.5 GHz, which is suitable for medium/long range search radars was chosen as detection pulse. A rectangle scatterer S1 modeled with 4 scattering points $(-0.6m, 0.7m)$, $(-0.55m, 0.7m)$, $(-0.5m, 0.7m)$, $(-0.45m, 0.7m)$ was chosen as an extended target, and a scatterer S2 modeled with one scattering point $(0m, 0.45m)$ was employed as a point-like target, as shown in Fig. 1. It is worth mention that four transceivers were employed for simplicity. The specific positions of the transmitter and receiver of each transceiver are listed in Table 1. The standard noise is added to the echo signals.

Table 1: The specific locations of each transceiver in numerical experiment (unit: m)

	Transmitter's Location	Receiver's Location
Transceiver 1	X=-0.125, Y=0	X=-0.175, Y=0
Transceiver 2	X=-0.025, Y=0	X=-0.075, Y=0
Transceiver 3	X=0.075, Y=0	X=0.025, Y=0
Transceiver 4	X=0.175, Y=0	X=0.125, Y=0

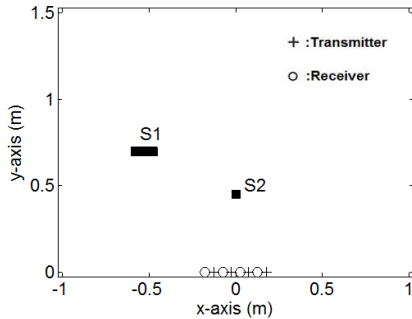


Fig. 1. Setup of the numerical experiment.

The sub-arrays are constituted in three ways, as shown in Table 2. In case 1, three sub-arrays are made, and each sub-array consists of two adjoining transceivers. In cases 2 and 3, two sub-arrays are got, and each sub-array consists of three adjoining transceivers in case 2, while there are two adjoining transceivers in case 3 whose total number of transceivers are three.

By using the proposed method, the results based on the aforementioned three cases are shown in Figs. 2 and 3. At SNR=0 dB, two targets can be distinguished obviously from all the detection maps. Precisely, the shapes and positions of this extended target and point-like target can be obtained, and there are hardly ghost images appearance in the detection maps. Moreover, compared with case 1 and case 2, although the imaging resolution of case 3 is a little declined, both the extended target and point-like target can be differentiated evidently, and these two targets are able to be detected easily. Investigate its germ, on the one hand, the increase of transceivers contained in each sub-array can improve the

TR-focusing effort; on the other hand, according to Equation (9), the increase of sub-arrays can enhance the pixel value at target's location due to the superposition that reduces the influence of noise. Thus, cases 1 and 2 are able to remove the artifacts better, compared with case 3.

Furthermore, when the SNR drops to -10 dB, two targets including shapes and locations are still able to be distinguished in all cases by using the proposed algorithm. And also compared with cases 1 and 2, the imaging resolution decreases a little, the reason is the same as discussed above. Moreover, the target images are not influenced by noise, while the images created by the background are influenced by noise dramatically. Thus, this method can suppress noise effectively.

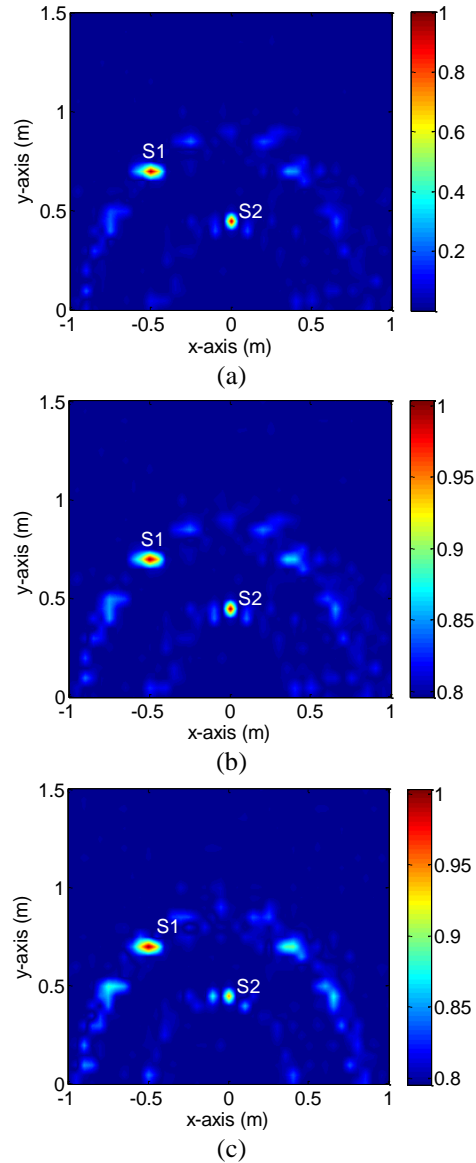


Fig. 2. Detection results based on various constitutions of the sub-arrays at SNR=0 dB: (a) Case 1, (b) Case 2, and (c) Case 3.

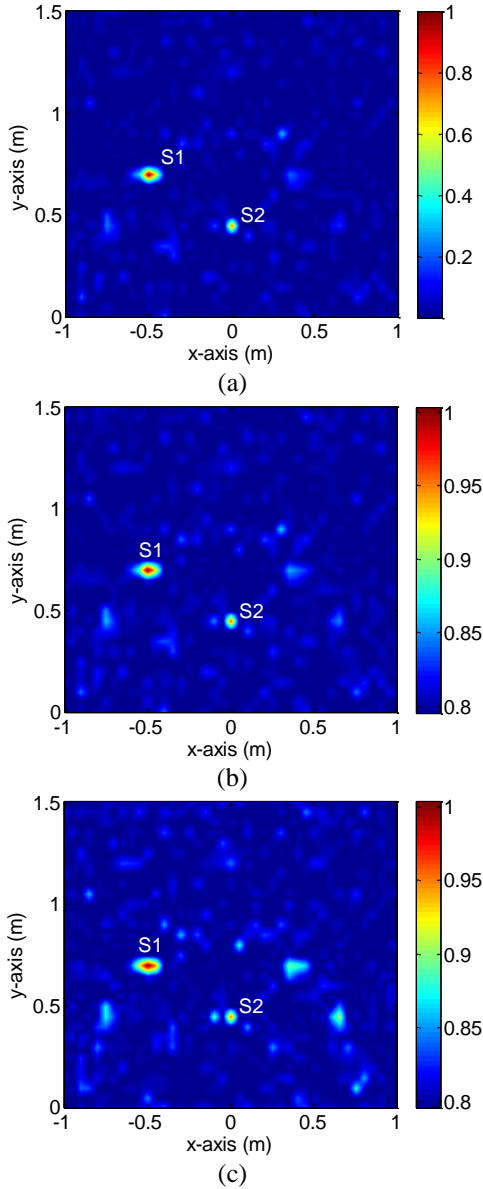


Fig. 3. Detection results based on various constitutions of the sub-arrays at SNR=-10 dB: (a) Case 1, (b) Case 2, and (c) Case 3.

Table 2: The constitution of the sub-arrays in numerical experiment

	Case 1	Case 2	Case 3
Sub-array 1	Transceiver 1 Transceiver 2	Transceiver 1 Transceiver 2 Transceiver 3	Transceiver 1 Transceiver 2
Sub-array 2	Transceiver 2 Transceiver 3	Transceiver 2 Transceiver 3 Transceiver 4	Transceiver 2 Transceiver 3
Sub-array 3	Transceiver 3 Transceiver 4		

B. Measured experiment

In this experiment, to evaluate the impact of using few echo signals on the performance of the proposed method, three transceivers were employed to obtain three echo signals. And these three transceivers are separated into two sub-arrays according to case 3 of Table 2.

The measured experimental setup is illustrated in Fig. 4, which is a 2-D construct. A cylinder metal pot whose diameter is 15cm was centered at (0m, 0.295m), and used as the scatterer. Three transceivers were used to detect the scatterer. Specific positions of the transmitting and receiving antennas of each transceiver are listed in Table 3. The Gaussian modulated pulse used in numerical experiment was also employed in this measured experiment.

Table 3: Specific positions of the transmitting and receiving antennas of each transceiver (unit: m)

Transceiver	Transmitting Antenna's Position	Receiving Antenna's Position
1	$x=-0.125, y=0$	$x=-0.175, y=0$
2	$x=0.025, y=0$	$x=-0.025, y=0$
3	$x=0.175, y=0$	$x=0.125, y=0$

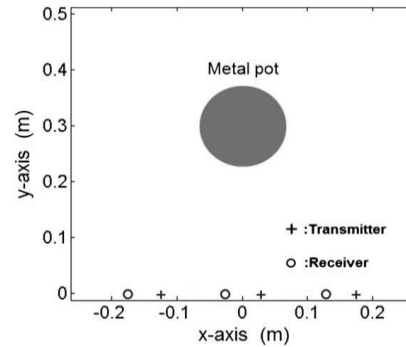


Fig. 4. Setup illustration of measured experiment.

The schematic diagram and the corresponding photo of the measured experimental are shown in Figs. 5 (a) and 5 (b). In each transceiver's location, the probing signal from a Tektronix AWG 7122B arbitrary waveform generator was amplified and used to drive a directional vivaldi antenna whose maximum direction of radiation is toward metal pot, and bandwidth is from 0.8 GHz to 8 GHz. The echo signal was received by an omnidirectional bow-tie antenna which has a bandwidth ranging from 2 to 12 GHz and recorded by Tektronix DSA 72004B.

I considered to process the echo signals in two cases, namely, the low-noise case and the high-noise case. In the low-noise case, the echo signals received by transceivers were processed directly. However, in the high-noise case, an extra noise was added to the realistic echo signals to achieve a SNR of -10 dB, where the SNR

was defined as the ratio between the amplitude of realistic echo signals and the standard deviation of the noise amplitude, and then the new signals were acquired. The results obtained by using the conventional TR algorithm and the proposed algorithm in the both cases are shown in Figs. 6 and 7, respectively.

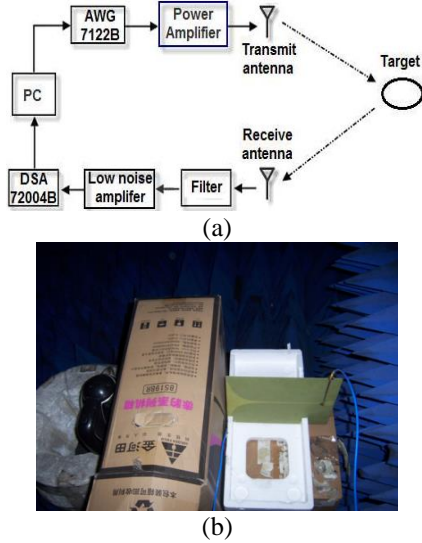


Fig. 5. Schematic diagram and photo of the measured experiment: (a) schematic diagram and (b) photo.

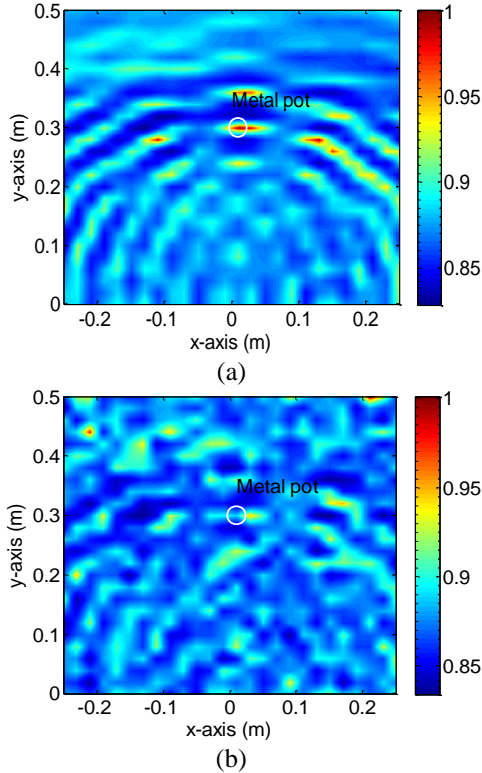


Fig. 6. Detection results by using the conventional TR algorithm in both cases: (a) low-noise and (b) high-noise.

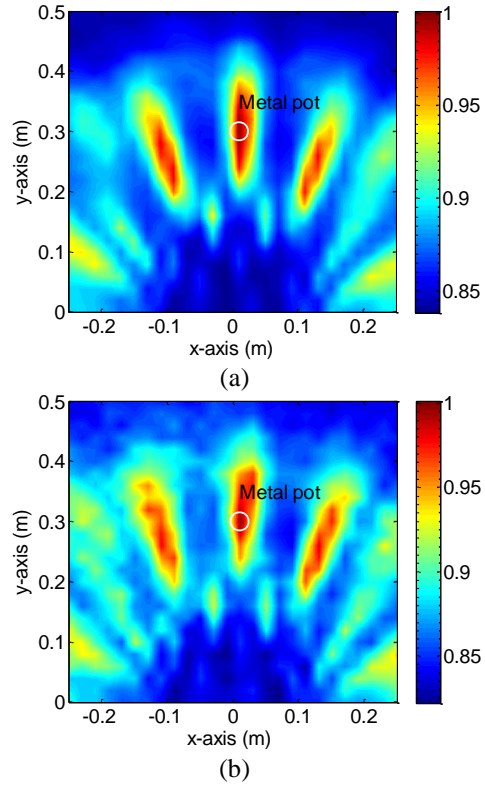


Fig. 7. Detection results by using the proposed algorithm in both cases: (a) low-noise and (b) high-noise.

Shown in Fig. 6 are detection results constructed by using the conventional TR algorithm. In low-noise case, the obtained image clearly reveals the correct target supports. The beneficial effect quickly disappeared, however, after adding noise. In high-noise case, the strong noise leads to several ghost images whose pixel values even exceed the pixel value in target's location. Clearly, Fig. 6 (b) is not an accurate reconstruction of the target's position. Such degradation performance is most likely a result of using few echo signals in the TR system.

Compared with Fig. 6, Fig. 7 can give a good idea of the scatterer's position in both situations. It can be seen that the detection maps based on the proposal method are not almost influenced by the enhancement of noise. Those mean the proposed algorithm outperforms the conventional TR method under few echo signals and strong noise interference conditions.

In order to facilitate comparison, the distributions of the maximum pixel values based on the two detection methods in both cases are able to be extracted from Fig. 6 and Fig. 7 and are also listed in Table 4. It can be found that the image peaks based on the proposal method appear at the same position that is the scatterer's location. In contrast, the conventional TR algorithm can point out the scatterer's location in the low-noise case, the maximum pixel value shifts to wrong position when noise enhances.

Table 4: The distributions of the maximum pixel values (unit: m)

	High-noise	Low-noise
The proposal algorithm	x=0.01,y=0.3	x=0.01,y=0.3
The conventional TR algorithm	x=0.21,y=0.5	x=0.01,y=0.3

In general, the decrease of the number of echo signals can weaken the TR-focusing effect, so that the peak of noise can exceed the peak of focusing signal under strong noise conditions. Therefore, the conventional TR algorithm which reconstructs the detection map by using the amplitude of TR signal at the focusing time, leads to a false image. However, since the proposal method utilizes the signal waveform similarity to reconstruct the detection map, the interference of strong noise is suppressed effectively. Thus, the target can be detected accurately by taking advantage of the proposed method, even under the situation of strong noise.

Otherwise, the number of each sub-array's transceivers and the number of sub-arrays can be increased by adding employed transceivers. Both of them can improve the performance of the proposed method, as mentioned before. Therefore, the proposed method can work better when the number of employed transceivers are more than three. Additionally, TR-MUSIC and DORT cannot be applied in the experiment, since their MDM whose size is 3×3 , cannot be constructed just by using 3 echo signals [5-8].

IV. CONCLUSIONS

In this paper, a novel TRD algorithm which uses the cross-correlation character of TR signals as the detection function is presented. Since the noise is irrelevant to TR-focusing signal, the proposal algorithm can effectively suppress the interference of noise, even in a situation where few echo signals are available. The result shows that the new method can utilize only three echo signals to distinguish the scatterer's location even under a SNR of -10 dB condition. Thus, compared with the conventional TR method, the proposed TRD algorithm is shown to be both practical and exploitable.

REFERENCES

- [1] Y. Song, N. Guo, and R. C. Qiu, "Implementation of UWB MIMO time-reversal radio testbed," *IEEE Antennas Wireless Propag. Lett.*, vol. 10, pp. 796-799, 2011.
- [2] B. B. Wang, Y. L. Wu, F. Han, et al., "Green wireless communications: a time-reversal paradigm," *IEEE J. Sel. Areas Commun.*, vol. 29, pp. 1698-1710, 2011.
- [3] S. Ding, B. Z. Wang, G. D. Ge, and D. S. Zhao, "Sub-wavelength array with embedded chirped delay lines based on time reversal technique," *IEEE Trans. Antennas Propag.*, vol. 61, pp. 2868-2873, 2013.
- [4] X. F. Liu, B. Z. Wang, S. Q. Xiao, and S. J. Lai, "Post-time-reversed MIMO ultrawideband transmission scheme," *IEEE Trans. Antennas Propag.*, vol. 58, pp. 1731-1738, 2010.
- [5] Y. Labyed and L. J. Huang, "Super-resolution ultrasound imaging using a phase-coherent MUSIC method with compensation for the phase response of transducer elements," *IEEE Trans. Ultrason. Ferroelectr. Freq. Control.*, vol. 60, pp. 1048-1060, 2013.
- [6] M. D. Hossain, A. S. Mohan, and M. J. Abedin, "Beamspace time-reversal microwave imaging for breast cancer detection," *IEEE Antennas Wireless Propag. Lett.*, vol. 12, pp. 241-244, 2013.
- [7] Y. Labyed and L. J. Huang, "Ultrasound time-reversal MUSIC imaging with diffraction and attenuation compensation," *IEEE Trans. Ultrason. Ferroelectr. Freq. Control.*, vol. 59, pp. 2186-2200, 2012.
- [8] X. F. Liu, B. Z. Wang, and J. L. Li, "Transmitting-mode time reversal imaging using MUSIC algorithm for surveillance in wireless sensor network," *IEEE Trans. Antennas Propag.*, vol. 60, pp. 220-230, 2012.
- [9] T. J. Ulrich, M. Griffo, and B. E. Anderson, "Symmetry-based imaging condition in time reversed acoustics," *J. Appl. Phys.*, vol. 104, pp. 1-8, 2008.
- [10] W. Liu and W. S. Lin, "Additive white Gaussian noise level estimation in SVD domain for images," *IEEE Trans. Image Process.*, vol. 22, no. 3, pp. 872-883, 2013.
- [11] L. Borcea, G. Papanicolaou, and C. Tsogka, "Theory and applications of time reversal and interferometric imaging," *Inverse Prob.*, vol. 19, pp. S139-S164, 2003.